Nanometrology optical ruler imaging system using diffraction from a quasiperiodic structure

Norimasa Yoshimizu*, Amit Lal, and Clifford R. Pollock

SonicMEMS Laboratory, School of Electrical and Computer Engineering, Cornell University, Ithaca, NY 14853, USA
**ny22@cornell.edu*

Abstract: This work demonstrates wafer-scale, path-independent, atomically-based long term-stable, position nanometrology. This nanometrology optical ruler imaging system uses the diffraction pattern of an atomically stabilized laser from a microfabricated quasiperiodic aperture array as a two-dimensional optical ruler. Nanometrology is accomplished by cross correlations of image samples of this optical ruler. The quasiperiodic structure generates spatially dense, sharp optical features. This work demonstrates new results showing positioning errors down to 17.2 nm over wafer scales and long term stability below 20 nm over six hours. This work also numerically demonstrates robustness of the optical ruler to variations in the microfabricated aperture array and discretization noise in imagers.

OCIS codes: (120.3940) Metrology; (050.1940) Diffraction.

References and links

1. N. Yoshimizu, A. Lal, and C. R. Pollock, "MEMS Diffractive Optical Nanoruler Technology for Tip-Based Nanofabrication and Metrology," in *Proceedings of the IEEE MEMS* (Institute of Electrical and Electronics Engineers, New York, 2009), pp. 547–550.
2. N. Yoshimizu, A. Lal, and C. R. Pollock, "Nanometrology Using a Quasiperiodic Pattern Diffraction Optical Ruler," J. Microelectromech. Syst. **19**(4), 865–870 (2010).
3. J. W. Goodman, *Introduction to Fourier Optics* (Roberts & Company Publishers, Greenwood Village, CO, 2005).
4. D. Robinson, and P. Milanfar, "Fundamental performance limits in image registration," IEEE Trans. Image Process. **13**(9), 1185–1199 (2004).
5. M. Tanibayashi, "Diffraction of light by quasi-periodic gratings," J. Phys. Soc. Jpn. **61**(9), 3139–3145 (1992).
6. R. D. Diehl, J. Ledieu, N. Ferralis, A. W. Szmodis, and R. McGrath, "Low-energy electron diffraction from quasicrystal surfaces," J. Phys. Condens. Matter **15**(3), R63–R81 (2003).
7. N. Ferralis, A. W. Szmodis, and R. D. Diehl, "Diffraction from one- and two-dimensional quasicrystalline gratings," Am. J. Phys. **72**(9), 1241–1246 (2004).
8. R. K. P. Zia, and W. J. Dallas, "A Simple Derivation of Quasi-Crystalline Spectra," J. Phys. Math. Gen. **18**(7), L341–L345 (1985).
9. V. Elser, "The Diffraction of Projected Structures," Acta Crystallogr. A **42**(1), 36–43 (1986).
10. F. Gähler, and J. Rhyner, "Equivalence of the Generalized Grid and Projection Methods for the Construction of Quasiperiodic Tilings," J. Phys. Math. Gen. **19**(2), 267–277 (1986).
11. D. Levine, and P. J. Steinhardt, "Quasicrystals. I. Definition and structure," Phys. Rev. B Condens. Matter **34**(2), 596–616 (1986).
12. J. E. S. Socolar, and P. J. Steinhardt, "Quasicrystals. II. Unit-cell configurations," Phys. Rev. B Condens. Matter **34**(2), 617–647 (1986).
13. C. Janot, *Quasicrystals: A Primer* (Cambridge University Press, Oxford, 1997).
14. M. Senechal, *Quasicrystals and Geometry* (Cambridge University Press, Oxford, 1995).
15. N. G. de Bruijn, "Algebraic theory of Penrose's non-periodic tilings of the plane I & II," Ned. Akad. Wetensch. Proc. Ser. A **43**, 39–66 (1981).

1. Introduction

Tip-based nanofabrication, such as dip-pen writing or thermal surface modification, is a promising technology that will enable future computational and sensor/actuator technologies. In addition, scanning probe microscopy is critical to semiconductor device process characterization and development as future electronic transistors are scaled to tens of nanometers. However, the success of nanoscale devices utilizing tip-based nanofabrication or

#133016 - $15.00 USD Received 10 Aug 2010; revised 8 Sep 2010; accepted 9 Sep 2010; published 16 Sep 2010

scanning probe metrology will rely critically on fast, precise, and long-term stable nanometrology of nanoscale features at length scales varying up to seven orders of magnitude. State-of-the-art capacitive sensors and strain sensors lack long travel range, and high precision optical encoders require a large reflective block which limits the frequency of movement. The resulting technological roadblock is the inability for a scanning probe microscope to quickly return to the same location after moving distances as large as tens of microns, much less an entire wafer. Consequently, time is laboriously spent searching for nanoscale features, limiting the throughput of nano-science and technology.

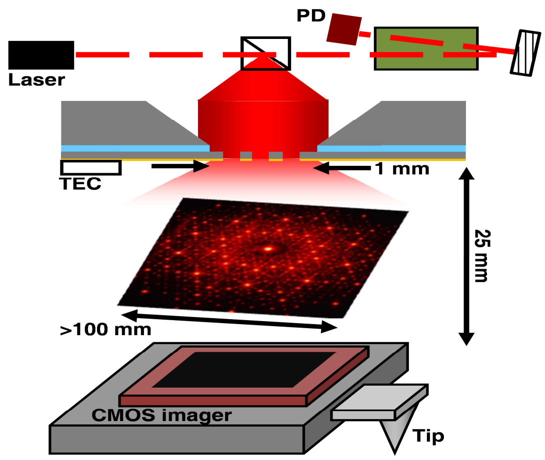

Fig. 1. Nanometrology Optical Ruler Imaging System schematic: An external cavity laser is frequency stabilized within 6 MHz, or a relative accuracy of 1.5×10^{-8}, to a saturated resonance (F = 2 to 1) of the D2-line of ^{85}Rb. A 22.77 ± 0.03 °C temperature stabilized microfabricated Penrose vertices grating diffracts the laser beam (fabricated using ebeam lithography on SOI device layer; device layer Si etch; through carrier wafer backside KOH etch; buffered HF release; Ti/Au evaporation). A wafer-scale optical ruler is shown. Tip/CMOS imager is mounted on a commercial stage. Upsampled Fourier transform cross correlation calculates the CMOS imager position within the optical ruler.

A basic idea for the Nanometrology Optical Ruler Imaging System (NORIS) was presented earlier [1]. NORIS uses an atomically stabilized laser as a stable base for metrology. The laser wavelength can be stabilized down to parts per billion over long times by locking the laser to an alkali atom absorption feature, as is similarly done in atomic clocks. The wavelength-stabilized laser beam is diffracted by a micropatterned metal thin film grating, which projects a diffraction pattern over the wafer-scale workspace and acts as a precise, accurate, and stable optical ruler. Using a quadrature photodiode, an analogue proportional-integral-differential control loop was used to position the photodiode on the center of peak in the optical ruler. Marks were made in poly(methyl methacrylate) at points corresponding to the optical ruler. The work resulted in a precision of $\pm 3 \times 10^{-4}$ precision over a 75 mm wafer.

However, the earlier implementation used a periodic grating aperture array, resulting in a hexagonal lattice diffraction optical ruler. In this work, a quasiperiodic pattern is used in the diffraction grating, which generates denser features than periodic or randomly generated patterns. Using such a pattern yields much greater precision than using a periodic structure. The system is described in detail elsewhere [2], but we show a schematic for recall in Fig. 1. This work demonstrates stability of 20 nm over six hours and precision down to 17 nm. We numerically demonstrate the robustness of the precision against low resolution analog-to-digital conversion of the image sampling, and against defects or variations in the microfabricated quasiperiodic aperture array.

#133016 - $15.00 USD Received 10 Aug 2010; revised 8 Sep 2010; accepted 9 Sep 2010; published 16 Sep 2010

2. Quasiperiodic diffraction

The optical ruler is generated by the diffraction of an atomically stabilized laser beam by a microfabricated metal thin film. In the far field, or Fraunhofer, diffraction region the amplitude of the diffracted optical field is given by,

$$U(x,y,z) = e^{ikz}/(i\lambda z) \times e^{ik\left(x^2+y^2\right)/2z} \times \iint_{\pm\infty} U(\xi,\eta)\exp\left[-i2\pi\left(x\xi + y\eta\right)/(\lambda z)\right] d\xi d\eta, \quad (1)$$

where the amplitude U is calculated at position (x,y,z) due to the diffraction of amplitude U at (ξ,η) by an optical field of wave vector k and wavelength λ [3]. The first factor decreases the optical power density as the optical field diffracts away from its origin. The second factor corresponds to a decrease in the optical field away from its center. The diffraction pattern will have more optical power towards the center of the image, and the optical power will generally decay towards the outer parts of the diffraction pattern. The double integral contains the information for the features in the diffraction pattern, a critical component in achieving high precision in NORIS.

The double integral in Eq. (1) is a Fourier transform of the amplitude U(ξ,η) at the diffraction plane. If the amplitude is constant across the aperture array, the double integral is a Fourier transform of the geometric shape of the aperture array where the openings are a constant intensity and the nontransmitting regions are zero. In order to maximize the precision of the NORIS system, a diffraction pattern, or optical ruler, is needed whereby image cross correlation techniques can be used to yield the highest precision in the estimates of displacement. The precision can be estimated based on the mean square error of the image registration at some offset **r** [4]. The lower bound of the mean square error is given by the Cramér-Rao bound,

$$MSE(\mathbf{r}) \geq J^{-1}(\mathbf{r}), \quad (2)$$

assuming an unbiased estimator, where the Fisher information matrix J is,

$$\left[J\left(\mathbf{r}\right)\right]_{ij} = -E[\partial^2(\log f)/(\partial \mathbf{r}_i \partial \mathbf{r}_j)], \quad (3)$$

which is the negative expectation value of the partial derivatives of the log of the likelihood function. Here, the likelihood function refers to the image registration, or the calculation of the translational offset of two images.

As might be expected, Eqs. (2) and (3) show that high precision in image registration will be achieved by using images with large amounts of image gradient. It is desired that the optical ruler contain image gradients that are unique across the whole image so that image registration will see high gradient features of different directions. This will result in high contrast in the cross correlation, resulting in higher image registration precision. Therefore, we are looking for a diffraction array that generates very dense, very sharp features across the optical ruler area. In addition, a diffraction pattern that is translationally asymmetric resulting in unambiguous positioning across a large area is desired.

An interesting solution can be found by considering different types of periodicity for the diffraction aperture arrays. To simplify the analysis, we consider one-dimensional diffraction. First, consider a periodic structure. The screen is opened periodically by an aperture of constant width, which in practice is constrained by fabrication limits. Therefore, the diffraction plane amplitude $U(\xi,\eta)$ is a periodic array of rect functions. As expected from the readily available analytical solution, the diffraction pattern or Fourier transform of the screen aperture is a sum of shifted sinc functions. The diffraction pattern is a number of peaks with a decaying, periodic envelope of the intensity which decays away from the center of the diffraction pattern. In Fig. 2, we show the one-dimensional diffraction pattern from a periodic, seven aperture screen. A Fourier transform is used to estimate the resulting diffraction pattern.

#133016 - $15.00 USD Received 10 Aug 2010; revised 8 Sep 2010; accepted 9 Sep 2010; published 16 Sep 2010

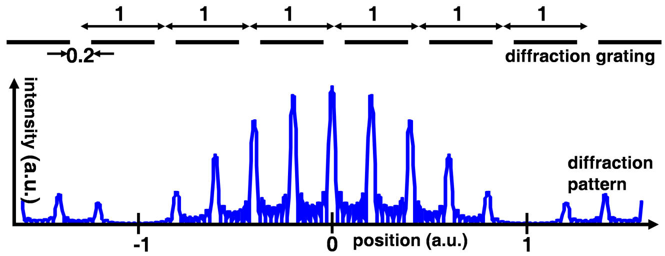

Fig. 2. One dimensional diffraction pattern from a seven element, periodic aperture array, estimated by a Fourier transform. The resulting pattern, a sum of sinc functions, results in evenly spaced peaks with an intensity envelope.

Figure 2 shows a number of peaks that are periodic, limited by the bandwidth of the aperture array. However, despite the spatial bandwidth available there are regions where there is an apparent lack of features: that is, having no optical gradient. We would like to decrease the mean square error of image registration shown in Eq. (2) by increasing the optical gradients across the one dimensional image. As a first attempt, randomness is introduced to the aperture array. Rather than periodically placing the apertures, their locations are randomly shifted. The resulting diffraction pattern is shown in Fig. 3. While some smaller intensity structure has appeared, there are number of large peaks that were clearly visible in the periodic case that have completely disappeared. The incoherent shifts in the aperture positions, i.e. white background noise, also slightly raises the noise floor of the diffraction pattern resulting in less signal-to-noise ratio of the peaks overall.

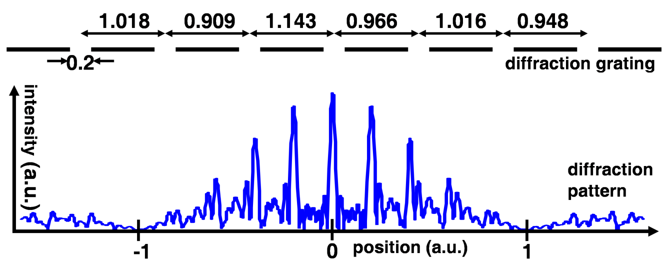

Fig. 3. One dimensional diffraction pattern from a seven element, aperiodic aperture array in an attempt to increase features in the diffraction pattern. The aperture positions are nearly periodic, located at slight displacements from their periodic locations in Fig. 2. Some low intensity structure appears to emerge, but some of the larger structures seen in the periodic case have disappeared.

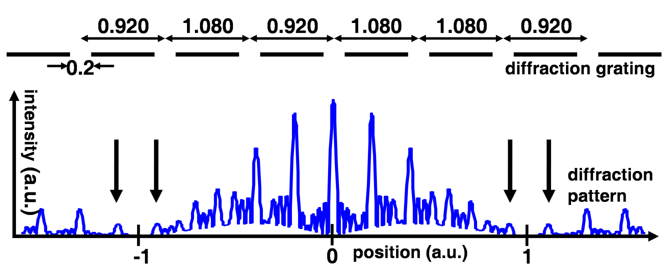

Fig. 4. One dimensional diffraction pattern from a seven element, quasiperiodic structure based on the Fibonacci sequence. Comparing this diffraction pattern to that in Fig. 2, we see that already several new peaks are introduced, some marked by arrows. The increase in sharp features increases the precision of NORIS.

Finally, we consider a quasiperiodic structure. Figure 4 shows the resulting one dimensional diffraction pattern from a quasiperiodic aperture array with equal bandwidth as the periodic case in Fig. 2. Rather than displacing the periodic structure by random shifts, they

#133016 - $15.00 USD Received 10 Aug 2010; revised 8 Sep 2010; accepted 9 Sep 2010; published 16 Sep 2010

are positioned based on the quasiperiodic Fibonacci sequence: see, for example [5–7]. Breaking the periodicity results in more frequency components in its composition, so that the resulting Fourier transform or diffraction pattern yields more peaks. Generally, quasiperiodicity involves incommensurate periods projected from higher dimensions, resulting in dense, sharp features in the corresponding Fourier transform: see, for example [8–15].

Although only seven apertures are used, the quasiperiodicity already introduces two new peaks per side in the diffraction pattern, as seen in Fig. 4. The introduction of new peaks in the diffraction pattern decreases the mean square error of image registration, as described in Eq. (2).

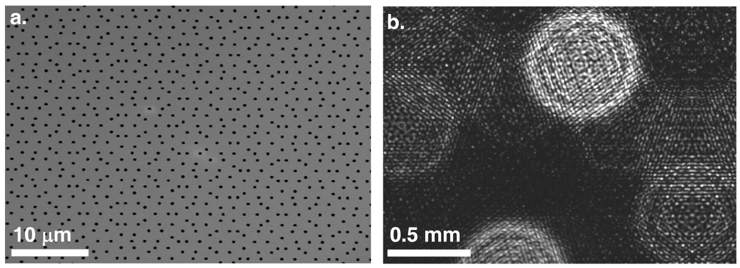

Fig. 5. a: Electron micrograph of a metal thin film quasiperiodic aperture array generated by using the vertices of a Penrose tiling. b: CMOS imager sample of the resulting diffraction pattern. Note the high density of sharp peaks, due to the diffraction from a quasiperiodic structure.

In NORIS, a two-dimensional quasiperiodic structure is required to generate the diffraction optical ruler. We use the quasiperiodic Penrose tiling of the plane using thin and thick rhombuses whereby aperture circles are placed at the vertices of the tiling [11]. The aperture array and the resulting diffraction pattern are shown in Fig. 5. Note the high density of peaks in the diffraction pattern, a result of the quasiperiodicity of the location of the apertures.

3. Experimental results

To demonstrate empirical results of NORIS, a 640 × 480, 2.2 μm pixel CMOS imager was mounted on a custom-made PC board, which was then attached to a piezoflexural stage. This commercial stage was integrated with short range, high precision capacitive sensors (nPoint NPXYZ100B). The stage is positioned 25.4 mm from the diffraction grating (along the longitudinal axis), and the imager located 50 mm from the center of the diffraction pattern (radial distance). The stage position measured by the capacitive sensors was compared to that detected by NORIS. First, a reference image of the optical ruler was sampled. Then the stage was moved and another image was sampled. The upsampled cross correlation between the reference and sample image calculates the absolute displacement of the stage. Figure 6 shows that over a 3 μm total displacement, NORIS demonstrated 17.2 nm mean absolute deviation. The bottom portion shows the residual. Figure 7 shows the stability of NORIS over 6 hours, at less than 20 nm. This long term stability is possible due to the atomically-based stability in the laser frequency. The optical ruler extends over several inches, resulting in a relative positioning error of 20 nm / 100 mm = 2×10^{-7}.

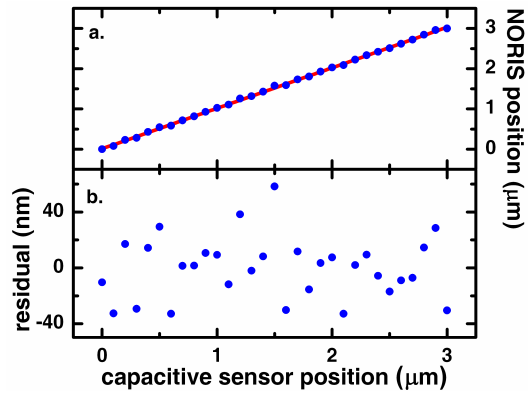

Fig. 6. NORIS positioning errors across 3 μm displacement, compared to short range, high precision capacitive sensor in a piezoelectric flexural stage.

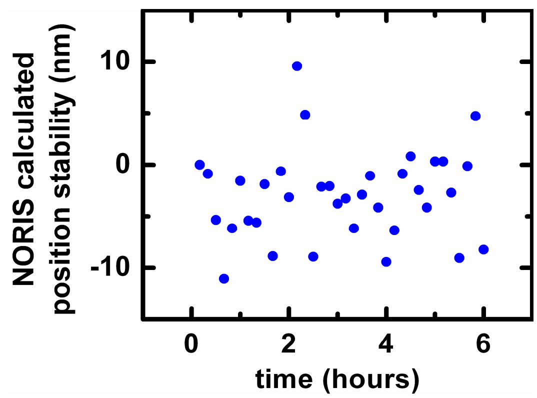

Fig. 7. NORIS positioning errors across over six hours.

4. Imager bit resolution

Previous NORIS data has been demonstrated using a modest CMOS imager with only 8-bit analog to digital conversion, a quantization error of tenths of percents. It was presumed that such a high quantization error would result in poor sampling of the optical ruler, and therefore poor precision in NORIS. Therefore, a gain sweep method was used to effectively sample the optical diffraction ruler at 14.6 bits, an improvement of two orders of magnitude, to improve the sampling of the quasiperiodic diffraction pattern.

However, we find that the precision in NORIS is very robust against high quantization errors. Lower bit resolutions are introduced by taking sampling images of the optical ruler and digitally sampling them at different bit resolutions. After the images are resampled at lower bit resolutions, they are again processed by the same cross correlation methods as before, and the resulting precision in NORIS can be compared at different bit resolution.

Figure 8 shows the effect of the bit resolution of a 640 x 480 imager on NORIS precision, using the empirical data presented in Fig. 6. The data at 14.6 bits matches the data in Fig. 6, but the other data reflect decreasing imager bit resolution. Bit resolutions of 9, 8, and 6 show equal performance. There is a slight linear drift at 4 bit resolution, and a large deviation at 3 bit resolution.

#133016 - $15.00 USD Received 10 Aug 2010; revised 8 Sep 2010; accepted 9 Sep 2010; published 16 Sep 2010

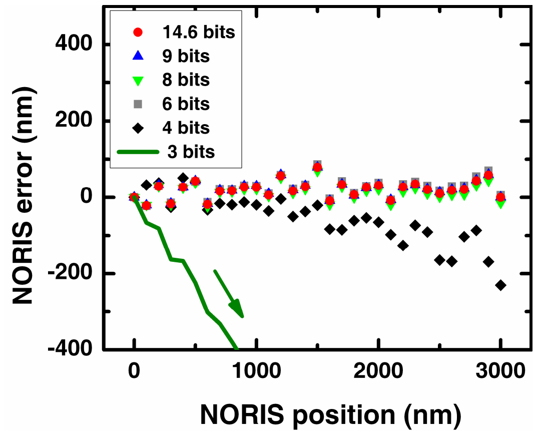

Fig. 8. Precision in NORIS affected by 640 × 480 imager bit resolution, using same data set as in Fig. 6. Resolution from 14.6 to 6 bits exhibit nearly identical performance. At 4 bits, a linear drift is induced and a large deviation is observed at 3 bit imager resolution. NORIS demonstrates great robustness against imager bit resolution.

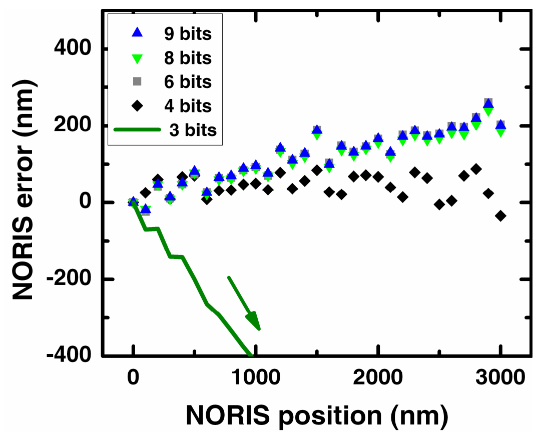

Fig. 9. Precision in NORIS affected by imager bit resolution as in Fig. 8, but with a reduced imager size of 576 x 432 pixels. Again, imager bit resolutions down to 6 exhibit the same precision, 4 bit resolution results in a linear drift, and finally at 3 bit resolution results in poor results.

In Fig. 9, a similar set of data is shown but with a reduced imager size of 576 x 432, a 10% reduction in the number of pixels per side from 640 x 480. Similar NORIS precision behavior is observed. Nearly identical NORIS precisions are shown for bit resolutions down to 6, a linear drift is observed at 4 bits, and finally at 3 bits the precision is poor. However, the high bit resolutions show a linear drift in NORIS suggesting that while NORIS very robust against bit resolution, it is not robust against the number of pixels of the imager.

#133016 - $15.00 USD Received 10 Aug 2010; revised 8 Sep 2010; accepted 9 Sep 2010; published 16 Sep 2010

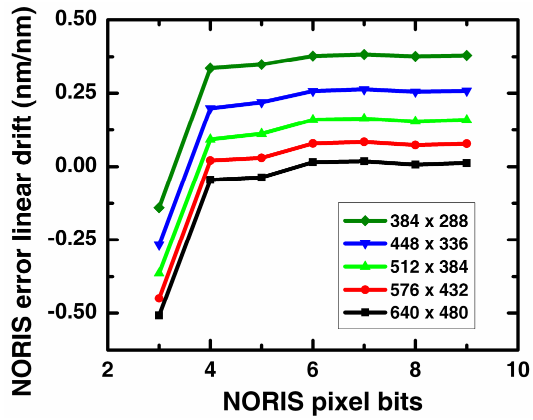

Fig. 10. Linear drift error in NORIS as the bit resolution is changed. Data shows robustness against orders of magnitude reduction in bit resolution, but shows significant linear drift error in NORIS as the number of pixels in the imager is decreased slightly.

This is confirmed by a comparison of NORIS linear drift error due to changes in the bit resolution and the number of pixels of the imager. Figure 10 shows the linear drift as the bit resolution is changed. As shown above, the bit resolution has little effect on the NORIS precision at all imager sizes, down to 4 to 6 bits. However, the Figure shows that the linear drift in NORIS strongly affected by the number of pixels in the imager. As the number of pixels per side of the imager is changed, the erroneous linear drift in NORIS increases significantly. For every 10% decrease in the number of pixels per side of the imager, there is approximately a 10% increase in the linear drift error of NORIS.

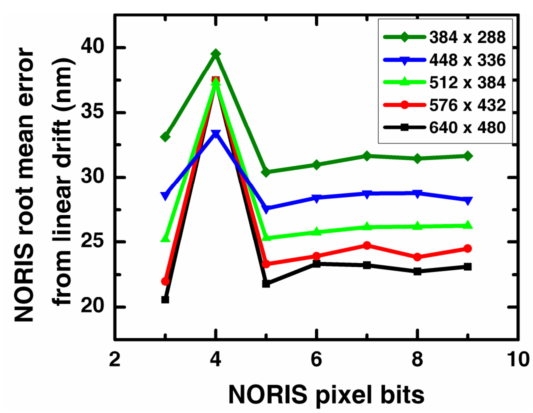

Fig. 11. Root mean error of NORIS about the linear drift described in Fig. 10. Again, the root mean error is constant through orders of magnitude reduction in bit resolution, but is sensitive to the number of pixels in the imager.

Similar results are show in Fig. 11 for the effect of bit resolution on the root mean error of NORIS about the linear drift described in Fig. 10. As the pixel bit resolution is reduced by orders of magnitude, the root mean error of NORIS remains constant. However, the root mean error of NORIS about the linear drift increases significantly as the number of pixels in the imager is reduced.

Figures 10 and 11 also show clearly that positioning errors increase as the number of pixels decreases. Intuitively, this is due to the decreased information regarding the image samples of the optical ruler. As is exploited in phase correlation methods for image registration, consider that the shift in the optical ruler image results in a $-k_x\Delta x - k_y\Delta y$ phase shift between the Fourier transforms of the two images. Calculating the displacement is a matter of calculating this phase gradient across the images, such as by using a linear

#133016 - $15.00 USD Received 10 Aug 2010; revised 8 Sep 2010; accepted 9 Sep 2010; published 16 Sep 2010

regression fit. As the number of pixels increase, the wave vectors k_x and k_y at which this gradient is calculated is increased, resulting in a better approximation of the displacement between the two images. At higher pixel numbers the gradient is sampled at smaller and smaller wave vectors which approximate the gradient more poorly, which may explain the reason why the marginal improvement in precision get smaller for higher numbers of pixels of the same size.

5. Aperture array variations

The data in Section 3 demonstrate that NORIS can achieve 17 nm precision. The positioning is performed 50 mm radially away from the center of the diffraction pattern. Towards the outer radius of the diffraction pattern the optical intensity decreases due to the second term in Eq. (1), the sizes of the features increases due to the finite size of the diffraction grating, and eventually the diffraction pattern completely disappears due to the finite coherence of the laser. These effects would result in increasingly poor precision. Therefore, within this 100 mm region the system can position itself within 17 nm of a desired position and demonstrates high precision.

Most applications of nanometrology require high precision. For example, a scanning probe or electron microscope would want to work within a 100 mm region of the wafer and be able to return precisely to the same transistor or photonic device for inspection. This affords the microscope a valuable capability. In most applications, the accurate distance between two devices is of little or no consequence. A transistor is not affected in performance if another transistor is 50 mm or 50 mm + 10 nm away in distance. The capability for a microscope or lithography tool to return consistently to the same device which is a valuable capability. Here we have demonstrated that NORIS can return to an arbitrary position, such as at a specific transistor, to within 17 nm anywhere within a 100 mm region.

However, wafer-scale positioning accuracy would provide two benefits. First, some current or future applications may require accurate wafer-scale positioning, such as for fabricating high coherence wafer-scale photonic systems. Second, accuracy is the conduit for nanometrology between tools, limited by the lowest accuracy. For example, a lithography tool and a microscopy tool must have enough accuracy so that transistors placed 50 mm + 10 nm apart can be fabricated and inspected at that distance, relying on the agreement of that distance between the two tools. A simple and common method for increasing accuracy would be to use a traceable calibration sample to measure standard lengths using the metrology tool. This would not require accuracy in NORIS per se, but with the high precision already demonstrated provides a straightforward way of matching the accuracy of the calibration sample, and would calibrate NORIS for long range accuracy. However, while it is an increasingly difficult challenge, inherent accuracy in the system would provide a valuable capability.

The basis for the stability for NORIS comes from the atomically stable frequency of the laser beam that is diffracted. By using saturation spectroscopy, for example, the laser frequency can be stabilized down to parts per billion which corresponds to nanometers over a six or twelve inch wafer. However, the accuracy of the positioning depends on the accuracy of the optical ruler. The image sampling clearly cannot directly calculate an image registration spanning wafer scale distances, unless the imager itself was that large. Instead, the imagers can be locally positioned accurately to the optical ruler and rely on the precise location of optical features within that optical ruler. This can be accomplished by using a set of calculated rather than sampled reference images of the optical ruler. Since the optical ruler diffracts a parts-per-billion stabilized laser, the stability of the optical wavelength should not be a significant problem.

There are number of factors that could affect the accuracy of the optical ruler. The angle of the incoming laser beam should remain perpendicular to the diffraction pattern. For example, the current 1 m path length of the incoming laser requires that the beam point within hundreds of nanometers of alignment. The size of the pixels in the imager would have to be known very well.

Here, we consider errors in the optical ruler caused by errors in the microfabricated aperture array. Mechanical stability data, previously and currently shown in this manuscript, have demonstrated that vibrational and temperature fluctuation effects are insignificant. For example, the aperture array is a thermally conductive thin film metal spanning only a millimeter. A large thermoelectric cooler can easily stabilize the temperature of such a small thermal load to within 0.03 °C. With thermal coefficients of expansion of parts per million and rigid support around structure, dynamic thermal changes are expected to remain in the parts or many parts per billion as required by NORIS.

There is, however, a dependency on the resulting diffraction optical ruler due to errors in the actual microfabrication of the aperture array. There are many possible sources for microfabrication errors in the aperture array. The sizes of the holes are nonuniform due to slight variations in etching rates and aspect ratios, mask exposure and development, etc. However, the diffraction pattern is a result of the sum of the amplitudes from all apertures which is expected to dilute the effect of small variations in the microfabrication of the aperture array. In addition, the Fourier transform of incoherent changes in the aperture array will tend to add white noise to the diffraction pattern, i.e. raise the noise floor, rather than change the peak structures within the optical ruler.

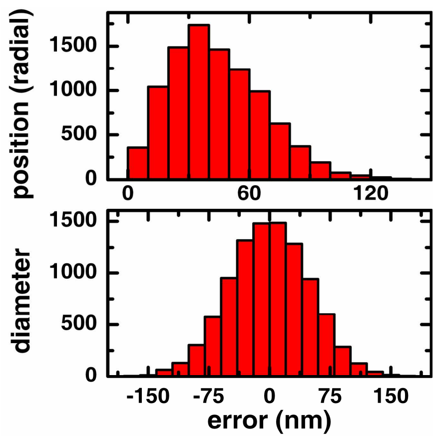

Fig. 12. Histogram of aperture diameter and radial positioning errors, for simulated errors of 50 nm in microfabrication.

To characterize the dependence of NORIS precision on variations in the aperture array, numerical simulations were carried out. A 780 nm optical plane wave was simulated to illuminate an aperture array of 9662, 3 μm holes spanning a millimeter in size placed at the vertices of a Penrose tiling, with a 10 μm length constant. This is the configuration shown in the electron micrograph in Fig. 5. The Fraunhofer diffraction at a distance of 25.4 mm is calculated. Sample image data sets were retrieved at a number of positions within the diffraction pattern, and those data sets were cross correlated to each other to calculate their displacement. The procedure is the same as the method used in NORIS. The calculated positions can be compared to their position within the diffraction pattern, which is know precisely by the simulation results. The aperture array is varied by both the position of the apertures and the diameter of the apertures, using a randomly generated normalized distribution. The aperture arrays were varied by their diameter and position offset of 20, 50, 100 and 500 nm; a sample histogram for 50 nm offset is shown in Fig. 12. Note that correlated errors, for example if the aperture arrays were stretched by 10 percent in one direction, are not considered. Such as in linear encoders that are fabricated with 275 nm steps rather than 250 nm steps, for example, unknown correlated errors are inevitably absorbed as a degradation of accuracy. In the case of diffraction as described by Eq. (1), errors in the scale of the aperture array leads to a proportional error in the scale of the optical ruler, as carried through the Fourier transform.

#133016 - $15.00 USD Received 10 Aug 2010; revised 8 Sep 2010; accepted 9 Sep 2010; published 16 Sep 2010

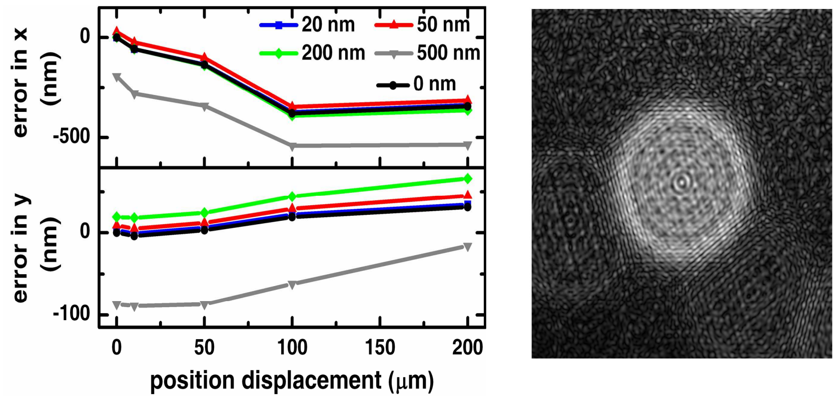

Fig. 13. NORIS positioning errors due to microfabrication errors. Positions are calculated by positioning NORIS based on image registration to error aperture array to zero error aperture array. Errors of up to 200 nm appear to have no impact on positioning error; a 500 nm fabrication error shows an effect on NORIS positioning error. As an example, image shows calculated diffraction pattern from 20 nm errors.

The resulting position errors are shown in Fig. 13, using a 500 × 500, 1 μm pixel imager and displaced in x from 0 to 200 μm. The image shows an example calculated diffraction pattern from 20 nm errors. Fabrication error is added to the aperture array, then the optical ruler image is registered to the image from a zero error aperture array. There is an inherent positioning error, even at zero fabrication error. This is a result of the cross correlation method which upsamples the Fourier transforms of the image. This results in errors because upsampling does not interpolate the image exactly. Microfabrication errors up to 200 nm appear to have little effect on the positioning, but microfabrication errors of 500 nm have a noticeable effect on NORIS precision. Therefore, the quasiperiodic diffraction optical ruler is robust to random errors in the aperture array. In addition to the demonstrated high precision, NORIS is accurate and thus can use a numerically calculated optical ruler to determine its position, and can tolerate large variations in the aperture array over time.

5. Conclusion

The current limit of precision could be caused by a number of direct or propagated sources of error. Directly, vibrations in the stage or optics cause an equivalent error in the positioning. Although the optical table is very stable, the PC board which holds the imager is mechanically the least stable and can decrease the precision. The thermal coefficient of expansion of materials used in the system such as aluminum or steel are on the order of tens of ppm per degree Kelvin, which could very well cause errors in positioning though the system is enclosed in an acoustically and thermally isolated miniature clean environment. Other sources of error can propagate throughout the system as proportional errors, such as laser wavelength error which causes a change in the scaling of the optical ruler. The laser wavelength stability of 1.5×10^{-8} is the base error of the system, and each component or source of error is added until the resulting 2×10^{-7} that we observe. The optical processing also affects the precision, such as if the individual pixel gain or analog to digital conversion are unstable, which in turn causes errors in the cross correlation image registration. The optical ruler has a spatial bandwidth of approximately 10 μm, for which an error of 20 nm would be a 0.1% error in the pixel intensity, or a substantial error of half a least significant bit on the 8-bit gain control of the imager. It is most likely that the current 17 nm limit we observe is due to the mechanical stability of the optical components in the system. For example, a four inch object which changes temperature by 0.1 K will increase its total length by 100 nm at 10 ppm/K, which is a shift of 50 nm within a 50 mm region. Further improvements will require additional work to stabilize the environmental sources of noise.

#133016 - $15.00 USD Received 10 Aug 2010; revised 8 Sep 2010; accepted 9 Sep 2010; published 16 Sep 2010

We have demonstrated the high precision and stability of NORIS, a system for parallel, path-independent, wafer-scale high precision nanometrology for scanning probe microscopes and nanoresolution stages. We have also demonstrated the robustness of the system against bit resolutions of the imager down to 4 bits; sensitivity of the system to changes in the number of pixels of in the imager; and the robustness of the system against microfabrication variations in its quasiperiodic aperture array.

Acknowledgements

This work was generously funded by the DARPA/TBN program (N66001-08-1-2074) and microfabrication was performed, in part, at the Cornell Nano-Scale Science and Technology Facility.